ACS APPLIED MATERIALS & INTERFACES

Research Article

www.acsami.org

Efficient Triarylamine–Perylene Dye-Sensitized Solar Cells: Influence of Triple-Bond Insertion on Charge Recombination

Cancan Yan,[†,‡] Wentao Ma,[†] Yameng Ren,[†,‡] Min Zhang,*[,†] and Peng Wang*[,†]

[†]State Key Laboratory of Polymer Physics and Chemistry, Changchun Institute of Applied Chemistry, Chinese Academy of Sciences, Changchun, 130022, China

[‡]University of Chinese Academy of Sciences, Beijing, 100049, China

Supporting Information

ABSTRACT: We synthesize two new metal-free donor–acceptor organic dyes (**C266** and **C267**) featuring a *N*-annulated perylene block. Owing to the improved coplanarity of conjugated units as well as the prolonged conjugation upon inserting a triple bond between the triarylamine and perylene segments, the **C267** dye exhibits a slightly red-shifted absorption peak and an enhanced maximum molar absorption coefficient with respect to its reference dye **C266**, leading to an improved photocurrent output in dye-sensitized solar cells. However, the triple-bond introduction also brings forth an over 100 mV reduced open-circuit photovoltage owing to faster interfacial charge recombination, which presents a clear correlation with a reduced mean thickness of self-assembled dye layer on titania as revealed by X-ray reflectivity measurements. The **C266** dye, albeit with a relatively weaker light-harvesting capacity, displays a higher power conversion efficiency of 9.0% under the 100 mW cm^{-2}, simulated AM1.5G sunlight.

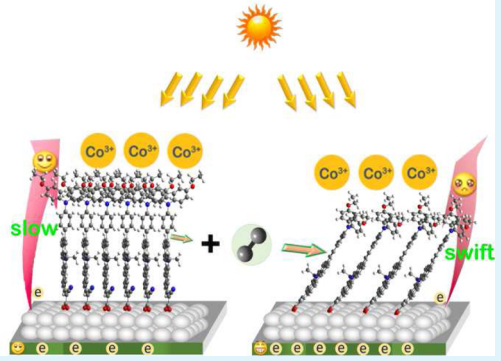

KEYWORDS: *solar cell, organic dye, perylene, charge recombination*

INTRODUCTION

The dye-sensitized solar cell (DSC) has been attracting intense research efforts in the background of questing for eco-friendly and low-cost technologies for solar energy utilization.[1] In the process of enhancing photovoltaic performance, molecular engineering of photosensitizing dyes is an unfailing research topic. A photosensitizer not only plays a pivotal role in determining the light-harvesting capacity, but also affects the microstructure of a self-assembled monolayer mainly consisting of dye molecules on the surface of titania nanocrystals to manage the multichannel interfacial charge-transfer kinetics. To date, ruthenium(II) polypyridine complexes, zinc porphyrin complexes, and thiophene-based organic dyes all present over 12% power conversion efficiencies (PCEs) at the air mass 1.5 global (AM1.5G) conditions.[2−4]

With a view to the resource restriction of ruthenium and the inferior stability of zinc porphyrin complexes, the development of metal-free donor–acceptor photosensitizers has caught more and more attention in past years owing to the availability of their raw materials, the flexibility of molecular design, the high molar extinction coefficient, and the bright color.[4−25] Recent studies have demonstrated that the utilization of rigid conjugated segment could have a favorable influence on the reduction of the energy gap and the suppression of radiationless excited-state deactivation stemming from the twisting motion of electronic skeleton.[26,27]

Perylene derivatives characteristic of coplanar and rigid electronic skeleton have been actively exploited as the building blocks of various optical and electrical materials,[28−31] owing to their thermal, chemical, and photostability. However, perylene as a building block of photosensitizers has only attracted moderate attention.[21,23,32−47] In this contribution, we first synthesize a new metal-free perylene dye (**C266**, Figure 1), featuring a triphenylamine electron donor, a *N*-annulated perylene π-linker, and a cyanoacrylic acid electron acceptor. Our preliminary theoretical calculations have shown that there is a large torsion angle between the triphenylamine and *N*-annulated perylene units. To resolve this issue, we further employ the strategy of inserting a triple-bond between two aromatic moieties[48−51] to construct another new dye (**C267**, Figure 1).

RESULTS AND DISCUSSION

The synthetic routes for the two new photosensitizing dyes are illustrated in Scheme 1. We first prepared the key intermediate **2** for both dyes in excellent yield via the regioselective monoformylation of *N*-annulated perylene bromide **1** by using the Vilsmeier–Haack reaction. Further performing the Suzuki–Miyaura cross-coupling of **2** and 4,4,5,5-tetramethyl-2-{4-[*N*,*N*-bis(4-hexyloxyphenyl)amino]phenyl}-1,3,2-dioxaborolane (**3**)[52] afforded one dye precursor **4** in good yield by employing a very active phosphine ligand, Sphos, developed by Buchwald

Received: October 21, 2014
Accepted: December 10, 2014
Published: December 10, 2014

 © 2014 American Chemical Society

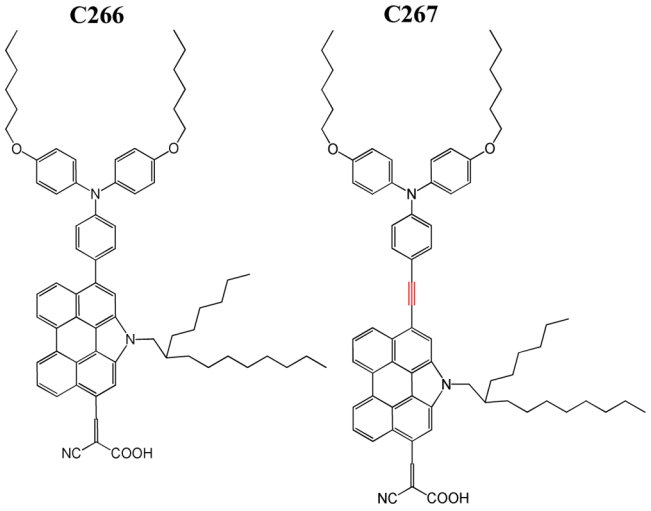

Figure 1. Chemical structures of the two new perylene dyes **C266** and **C267** studied in this work.

and his co-workers.[53] Finally the well-known Knoevenagel condensation was carried out to obtain the cyanoacrylic acid dye **C266**. On the other side, cross-coupling *N*,*N*-bis(4-hexyloxyphenyl)-4-iodoaniline (**5**)[52] with (triisopropylsilyl)-acetylene via the Sonogashira coupling gave the intermediate **6**, which then underwent desilication in the presence of tetra-*n*-butylammonium fluoride to yield compound **7** quantitatively. Subsequently, the intermediates **2** and **7** were cross-coupled via the Sonogashira coupling to produce the precursor **8** for the final dye construction of **C267** based on the same procedure for **C266**. For the synthetic details, see the Experimental Section.

Wide potential range cyclic voltammograms (Figure 2) of **C266** and **C267** dissolved in anhydrous tetrahydrofuran (THF)

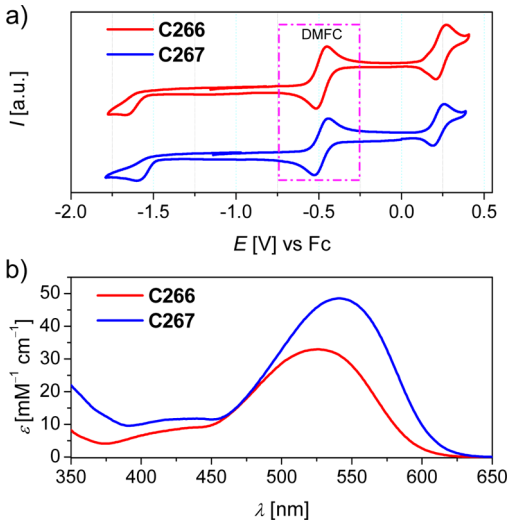

Figure 2. (a) Cyclic voltammograms of **C266** and **C267** in THF with 0.1 M 1-ethyl-3-methylimidazolium bis(trifluoromethanesulfonyl)-imide (EMITFSI) as the supporting electrolyte and decamethylferrocene (DMFC) as the internal reference. All potentials are reported against ferrocene (Fc). Working electrode: glassy carbon; counter electrode: Pt; reference electrode: Ag/Ag^+; scan rate: 5 mV s^{-1}. (b) Electronic absorption spectra of the 150 μM dye solutions in THF.

were recorded by placing a three-electrode electrochemical cell in a nitrogen-filled glovebox, to examine the influence of inserting a triple bond between the triphenylamine and perylene units upon the highest occupied molecular orbital

Scheme 1. Synthetic Routes for C266 and C267[a]

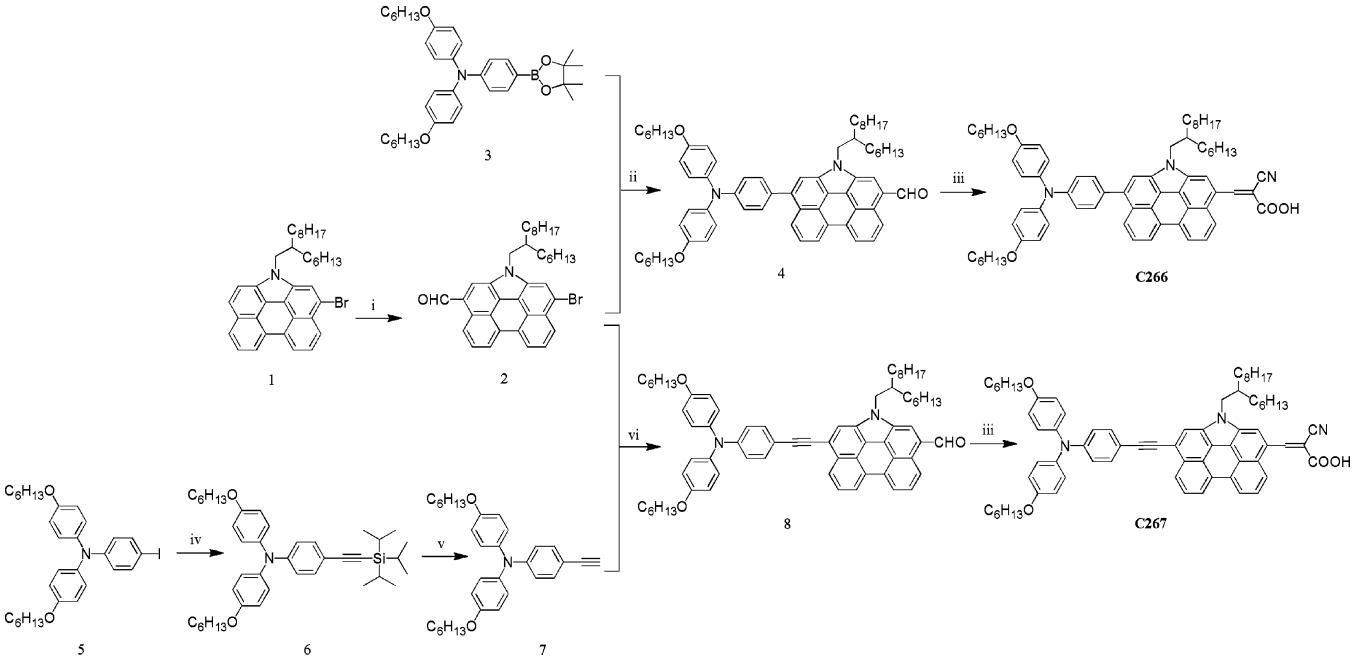

[a]Reagents and conditions: (i) DMF, $POCl_3$, DCE, 0 to 40 °C, 12 h; (ii) $Pd(OAc)_2$, Sphos, K_3PO_4, dioxane/H_2O (v/v, 5/1), reflux, 8 h; (iii) cyanoacetic acid, NH_4AC, $MeCN/CHCl_3$ (v/v, 1/2), reflux, 48 h; (iv) (triisopropylsilyl)acetylene, $Pd(PPh_3)_2Cl_2$, CuI, Et_3N, toluene, 80 °C, overnight; (v) tetra-*n*-butylammonium fluoride, CH_2Cl_2, RT, 3 h; (vi) $Pd(PPh_3)_2Cl_2$, CuI, Et_3N, toluene, 80 °C, overnight. Herein, C_6H_{13} and C_8H_{17} denote *n*-hexyl and *n*-octyl, respectively.

dx.doi.org/10.1021/am507261j | ACS Appl. Mater. Interfaces 2015, 7, 801−809

Table 1. Measured and Calculated Energy Levels, Energy-Gaps, and Electronic Absorption Properties of C266 and C267

dye	E_L^{CV} [a] [eV]	E_L^{DFT} [b] [eV]	E_H^{CV} [a] [eV]	E_H^{DFT} [b] [eV]	E_{H-1}^{DFT} [b] [eV]	$\Delta E_{L/H}^{CV}$ [a] [eV]	$\Delta E_{L/H}^{DFT}$ [b] [eV]	$\Delta E_{L/H-1}^{DFT}$ [b] [eV]	$\lambda_{abs,max}^{meas}$ [c] [eV]	$\lambda_{abs,max}^{TDDFT}$ [d] [nm]	$\epsilon_{abs,max}^{meas}$ [c] [mM^{-1} cm^{-1}]	f [d]	transition [d]
C266	−3.33	−2.91	−5.04	−5.08	−5.53	1.71	2.17	2.62	526	514	32.9	1.33	H→L (77%) H−1→L (23%)
C267	−3.39	−3.02	−5.01	−5.05	−5.57	1.62	2.03	2.55	540	549	48.5	1.86	H→L (85%) H−1→L (15%)

[a]Experimental frontier orbital energy levels (E_L^{CV} and E_H^{CV}) with respect to the vacuum reference are calculated via $E = -4.88 - eE_{onset}$, where E_{onset} is the onset potential (Figure 2a) of oxidation or reduction of the ground-state of a dye measured with cyclic voltammetry. H and L represent HOMO and LUMO, respectively. Energy-gap ($\Delta E_{L/H}^{CV}$) is calculated via $\Delta E_{L/H}^{CV} = E_L^{CV} - E_H^{CV}$. [b]Theoretical frontier orbital energy levels (E_L^{DFT}, E_H^{DFT}, and E_{H-1}^{DFT}) with respect to vacuum are computed with the DFT method at the B3LYP/6-311G(d,p) level for a dye in THF. Energy-gaps ($\Delta E_{L/H}^{DFT}$ and $\Delta E_{L/H-1}^{DFT}$) are calculated via $\Delta E_{L/H}^{DFT} = E_L^{DFT} - E_H^{DFT}$ and $\Delta E_{L/H-1}^{DFT} = E_L^{DFT} - E_{H-1}^{DFT}$. [c]$\lambda_{abs,max}^{meas}$ and $\epsilon_{abs,max}^{meas}$ were measured for a diluted THF dye solution. [d]$\lambda_{abs,max}^{TDDFT}$, f (oscillator strength), and the corresponding transition assignments were computed with the TDDFT method at the MPW1K/6-311G(d,p) level for a dye in THF.

(HOMO) and lowest unoccupied molecular orbital (LUMO) energy levels. The derived parameters were compiled in Table 1. It is found that the triple-bond insertion destabilizes the HOMO energy level (E_H^{CV}) from −5.04 to −5.01 eV with respect to the vacuum reference and stabilizes the LUMO energy level (E_L^{CV}) from −3.33 to −3.39 eV, generating a contracted LUMO/HOMO energy gap ($\Delta E_{L/H}^{CV}$) of 1.62 eV for **C267** in contrast to that of 1.71 eV for **C266**. Thereby, it is within expectation to observe a red-shifted maximum absorption wavelength ($\lambda_{abs,max}^{meas}$) of 540 nm for **C267** in comparison with that of 526 nm for **C266** shown in Figure 2b. Moreover, the maximum molar absorption coefficient ($\epsilon_{abs,max}^{meas}$) is augmented from 32.9 to 48.5 mM^{-1} cm^{-1} upon the triple-bond insertion.

We also resorted to quantum calculation with the density functional theory (DFT) and time-dependent density functional theory (TDDFT) methods to gain insight into the triple-bond insertion induced energy levels and absorption spectra. As listed in Table 1, DFT calculations can nicely simulate the relative alignments of HOMOs and LUMOs of these two dyes. In addition, our DFT calculation has disclosed a deeper HOMO of −5.16 eV for 4-ethynyl-*N*,*N*-bis(4-(hexyloxy)-phenyl)aniline in comparison with that of −5.03 eV for *N*,*N*-bis(4-(hexyloxy)phenyl)aniline. Therefore, the higher HOMO of **C267** with respect to that of **C266** can be ascribed to a more planarized electronic backbone as shown in Figure 3. **C266** possess a large dihedral angle of 49.7° between the phenyl and *N*-annulated perylene units due to the steric hindrance, while the corresponding dihedral angle in **C267** was nearly 0° along with the insertion of a triple-bond. This planarization could enhance the conjugation significantly. Moreover, TDDFT calculation can nicely mimic the experimentally measured red-shifting of absorption peak and the increase of absorption coefficient from **C266** to **C267**. The computed maximum absorption wavelength ($\lambda_{abs,max}^{TDDFT}$) and the corresponding oscillator strengths (f) for $S_0 \rightarrow S_1$ transition are also listed in Table 1. In general, the $S_0 \rightarrow S_1$ transitions to LUMO for both **C266** and **C267** are mainly originated from HOMO and HOMO−1. Nevertheless, the contribution from HOMO is obviously increased for **C267** (85%) in comparison with that of **C266** (77%) due to a better spatial overlap between HOMO and LUMO as illustrated in Figure 3. The $S_0 \rightarrow S_1$ absorptions of these two dyes manifests a strong charge-transfer transition characteristic. The smaller LUMO/HOMO energy gap ($\Delta E_{L/H}^{DFT}$), the smaller LUMO/HOMO−1 energy gap

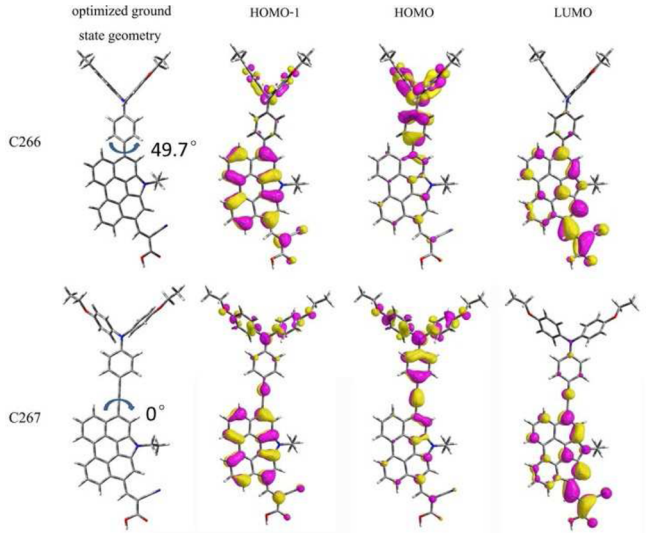

Figure 3. Optimized ground-state molecular geometries and the topologies of molecular orbitals involving the $S_0 \rightarrow S_1$ transitions of **C266** and **C267** in THF. The isodensity surface values are fixed at 0.03. To improve the computational efficiency, the large aliphatic substituents were replaced with ethyl.

($\Delta E_{L/H-1}^{DFT}$), and the stronger LUMO/HOMO electronic coupling of **C267** jointly dominate its red-shifted low-energy absorption peak with respect to **C266**. In addition, the more effective spatial overlap of the ground-state and excited-state wave functions of **C267** could also make a favorable contribution to the molar absorption coefficient enhancement as observed in absorption measurements (Figure 2b).

We further evaluated the impact of energy-gap diminution stemming from the triple-bond insertion on the wavelength-dependent light-harvesting efficiencies (ϕ_{lh}) of dye-grafted titania films, which was also immersed in a tris(2,2′-bipyridine) cobalt (Co-bpy) electrolyte. For its detailed composition, see the Experimental Section. In addition, by monitoring the small but reliable change of light absorption of a dye solution at a given volume, we have roughly estimated the loading amount (c_m) of dye molecules on the mesoporous titania film, which also has an important influence on the light-harvesting capacity in DSCs. It is found that there is a decreased c_m of 1.9×10^{-8} mol cm^{-2} μm^{-1} for **C267**, in contrast to that of 2.3×10^{-8} mol cm^{-2} μm^{-1} for **C266** (Supporting Information, Table S1).

dx.doi.org/10.1021/am507261j | ACS Appl. Mater. Interfaces 2015, 7, 801−809

However, the **C267** cell still presents higher ϕ_{lh} at the long wavelengths starting from 550 nm (Figure 4a), owing to

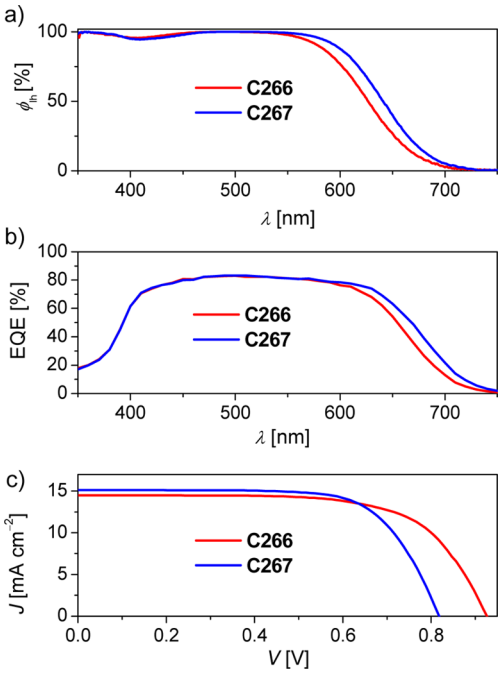

Figure 4. (a) Light-harvesting efficiencies (ϕ_{lh}) plotted vs wavelength (λ) for the 4.2 μm thick, dye-grafted mesoporous titania films immersed in a Co-bpy electrolyte for DSC fabrication. (b) External quantum efficiency (EQE) plotted against λ for cells made with a dye-grafted bilayer (4.2 + 5.0 μm thick) titania films in combination with a Co-bpy electrolyte. (c) Current−voltage (J−V) characteristics of cells measured under an irradiance of 100 mW cm^{-2}, simulated AM1.5G sunlight. An antireflection film was adhered to a testing cell during measurements. The aperture area of the employed metal mask is 0.160 cm^{-2}.

augmented molar absorption coefficients in this spectral region. The external quantum efficiencies (EQEs) of **C266** and **C267** in DSCs as a function of wavelength (λ) were further examined in combination with a bilayer titania film and a Co-bpy electrolyte. The cell fabrication details can be found in the Experimental Section. As depicted in Figure 4b, the EQE summits of both dyes are ~80%. The main difference lies in the spectral range from 600 to 750 nm, which is in good accord with light-harvesting measurements (Figure 4a).

The solar-to-electricity conversion efficiencies of these two dyes were further assessed by measuring the current−voltage (J−V) curves under an irradiance of 100 mW cm^{-2}, simulated AM1.5G sunlight. The average photovoltaic parameters of six cells are collected in Table 2. The **C266** cell possesses a short-circuit photocurrent density (J_{sc}) of 14.50 mA cm^{-2}, an open-circuit photovoltage (V_{oc}) of 928 mV, and a fill factor (FF) of 0.669, affording a PCE of 9.0%. This is the highest efficiency for peylene DSCs. In accord with the photocurrent predicted from EQEs, **C267** presents an improved J_{sc} of 15.13 mA cm^{-2}. However, the introduction of triple-bond brings forth a shrinking of over 100 mV in the V_{oc} value, from 928 mV to 819 mV, resulting in a relatively lower PCE of 8.6%.

For an unchanged redox electrolyte, it is well-recognized that the V_{oc} of a DSC under light is positively relevant to the electron quasi-Fermi-level ($E_{F,n}$) of a titania film, which is jointly determined by the titania conduction band edge (E_C) and electron density stored in titania.[54,55] Furthermore, the electron density in titania, at a certain flux of carrier photogeneration, is governed by the rate of charge recombination between photoinjected electrons with holes (the Co-bpy(III) ions) in the electrolyte and/or the oxidized dye molecules. Thus, we performed the charge extraction (CE) and small-pulse transient photovolatge decay (TPD) experiments to take a close look at the energetic and kinetic origins of the visible V_{oc} difference.[56,57] As Figure 5a shows, the **C267** cell

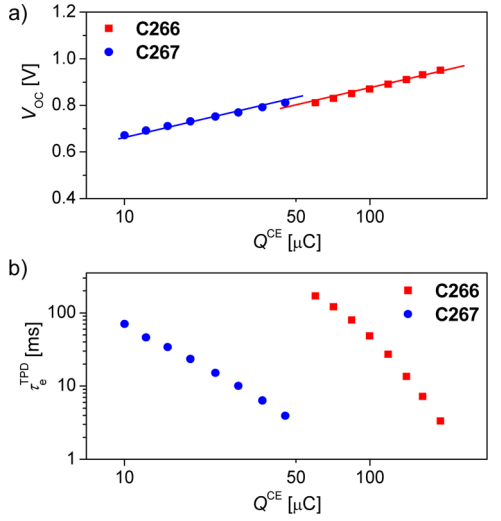

Figure 5. (a) Plots of charge stored in a dye-grafted titania film (Q^{CE}) measured with charge extraction (CE) method as a function of open-circuit photovoltage (V_{oc}). The solid lines are guides to eye. (b) Comparison of electron lifetime (τ_e^{TPD}) measured with the small-pulse transient photovoltage decay (TPD) method against Q^{CE}.

exhibits a less extracted charge (Q^{CE}) at the same V_{oc} or potential bias with respect to the **C266** cell, implying that the titania conduction-band edge in the **C267** cell moves up for ~40 mV with respect to the electrolyte Femi level ($E_{F,el}$). Note that the loading amount of **C267** on titania is smaller than that of **C266**. The uncovered titania could effectively interact with the electrolyte additive 4-*tert*-butylpyridine (*t*BP), which has a strong capacity of lifting the titania conduction-band edge.[58] The dye coverage related conduction-band edge shift observed here is in line with our previous study.[26] However, the up-shifted conduction-band edge does not lead to an improved V_{oc} due to an almost 2 orders of magnitude of the reduced lifetime of photoinjected electrons (τ_e^{TPD}) at a given Q^{CE} for the **C267** cell as described in Figure 5b. Note that, for the **C267** cell, the

Table 2. Averaged Photovoltaic Parameters of Six Cells Measured at an Irradiance of 100 mW cm^{-2}, Simulated AM1.5G Sunlight

dye	J_{sc}^{EQE} [mA cm^{-2}]	J_{sc} [mA cm^{-2}]	V_{oc} [mV]	FF	PCE [%]
C266	14.26 ± 0.04	14.50 ± 0.03	928 ± 3	0.669 ± 0.003	9.0 ± 0.2
C267	15.09 ± 0.05	15.13 ± 0.04	819 ± 5	0.693 ± 0.004	8.6 ± 0.1

dx.doi.org/10.1021/am507261j | ACS Appl. Mater. Interfaces 2015, 7, 801−809

stabilization of LUMO and the lifting of TiO_2 conduction-band edge do not lead to a lower EQE summit, which may be related to the prolonged excited-state lifetime for **C267** as depicted in Supporting Information, Figure S1.

The dark current−voltage curves were also surveyed to inspect the charge recombination. As depicted in Figure 6a,

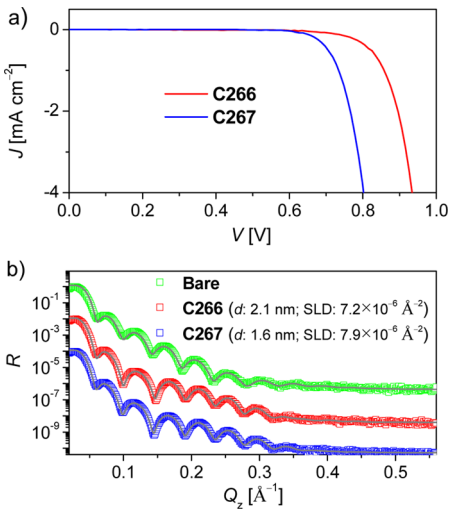

Figure 6. (a) J−V characteristics in the dark of the **C266** and **C267** cells. (b) Measured (symbols) and simulated (solid lines) XRR curves for the bare and dye-grafted titania films. R is the reflectivity and Q_z is the perpendicular momentum transfer. Each curve is offset by 10^{-2} with respect to the previous one for clarity. The derived thickness (d) and X-ray scattering length density (SLD) of a dye layer on titania are also included in the inset of panel b.

there is an obviously increased dark current for the **C267** cell at a given potential bias, suggesting an accelerated recombination of electrons in titania with the holes in electrolyte. For DSCs made with some medium-sized redox couples, the average thickness of dye layer on the surface of titania can impact the electronic coupling matrix elements between the electron in titania and the hole in electrolyte and, thus, affect the rate of interfacial charge-recombination reaction. Thereby, it could be highly necessary to obtain a basic understanding on microstructure of the dye layer on the titania surface. We carried out the X-ray reflectivity (XRR) measurements[59−61] on dye-grafted planar titania. The planar titania was predeposited via atomic layer deposition (ALD) on single-crystal silicon (110). A bilayer model was employed to fit the initial reflectivity profiles (Figure 6b) of dye-grafted ALD titania films, and the refined structural parameters were compiled in Supporting Information, Table S1. It is found that **C266** forms a thicker dye layer with a mean thickness (d) of 2.1 nm, compared to that of 1.6 nm for **C267**. It is interesting to note that the longer **C267** does not lead to an increased thickness of dye layer, implying a larger average title angle of the **C267** molecules on titania. This feature of thinner self-assembled dye layer for **C267** allows the cobalt(III) ions to locate in close proximity to titania, speeding up the interfacial charge recombination as aforementioned observation in TPD and dark current−voltage curve measurements. This lower V_{oc} of **C267** cell could be improved by employing the protocol of pinhole defect filling as presented in our previous work.[62]

CONCLUSIONS

In summary, we have synthesized two new perylene dyes characteristic of a coplanar *N*-annulated perylene block. The **C266** photosensitizer exhibits a good power conversion efficiency of 9.0% measured under the 100 mW cm^{-2}, simulated AM1.5G sunlight. The introduction of triple bond between the triarylamine and perylene segments can endow the dye molecule with a planar conjugated skeleton, leading to a narrower energy-gap and an improved molar extinction coefficient. The enhanced response to the red photons in the solar emission spectrum evokes an enhanced photocurrent output. However, the triple-bond insertion brings forth a reduced loading amount and a more tilted anchoring mode of dye molecules on the surface of titania. This feature of a self-assembled dye layer is well-associated with fast interfacial charge recombination and reduced photovoltage output. Our work has highlighted the important consideration of the interfacial microstructure in the future dye design and device engineering.

EXPERIMENTAL SECTION

Materials. Toluene, *N*,*N*-dimethylformide (DMF), phosphorus oxychloride ($POCl_3$), 1,2-dichloroethane (DCE), 1,4-dioxane, acetonitrile, chloroform, and triethylamine (Et_3N) were distilled before use. Palladium(II) acetate ($Pd(OAc)_2$), 2-(2,6-dimethoxybiphenyl)-dicyclohexylphosphine (Sphos), K_3PO_4, 2-cyanoacetic acid, ammonium acetate (NH_4Ac), (triisopropylsilyl)acetylene, bis-(triphenylphosphine)palladium(II) dichloride ($Pd(PPh_3)_2Cl_2$), copper(I) iodide (CuI), tetra-*n*-butylammonium fluoride, and decamethylferrocene (DMFC) were purchased from Sigma-Aldrich. 3-Bromo-1-(2-hexyldecyl)-1*H*-phenanthro[1,10,9,8-*cdefg*]carbazole (**1**),[63] 4,4,5,5-tetramethyl-2-{4-[*N*,*N*-bis(4-hexyloxyphenyl)amino]-phenyl}-1,3,2-dioxaborolane (**3**),[52] and 4-(hexyloxy)-*N*-(4-(hexyloxy)-phenyl)-*N*-(4-iodophenyl)aniline (**5**)[52] were synthesized according to the respective literature procedures. Other chemicals were purchased and used without further purification. The preparation details of **C266** and **C267** are described as follows.

10-Bromo-1-(2-hexyldecyl)-1*H*-phenanthro[1,10,9,8-*cdefg*]-carbazole-3-carbaldehyde (2). **1** (900 mg, 1.51 mmol) was dissolved in DCE (10 mL) in a three-neck round-bottom flask and cooled to 0 °C using an ice-salt bath. DMF (0.35 mL, 5.22 mmol) and $POCl_3$ (0.19 mL, 1.96 mmol) were added before the reaction mixture was stirred at 40 °C for 12 h. The saturated sodium acetate aqueous solution (10 mL) was added, and the resulting mixture was stirred for another 2 h. Then the mixture was extracted into dichloromethane, and the organic layer was washed with water and dried over anhydrous sodium sulfate. After removing solvent under reduced pressure, the residue was purified by column chromatography over silica gel with ethyl acetate/petroleum ether as eluent (v/v, 1/20) to afford a yellow oil as the desired product **2** (765 mg, 85% yield). ^{1}H NMR (400 MHz, $CDCl_3$) δ: 10.23 (s, 1H), 8.99 (d, J = 8.2 Hz, 1H), 8.20 (m, 2H), 8.05 (d, J = 8.2 Hz, 1H), 7.69 (m, 1H), 7.63 (m, 1H), 7.47 (m, 2H), 3.70 (d, J = 7.2 Hz, 2H), 1.81 (m, 1H), 1.13 (m, 24H), 0.81 (m, 6H). ^{13}C NMR (100 MHz, $CDCl_3$) δ: 192.59, 133.97, 129.98, 129.27, 128.94, 128.85, 127.23, 126.72, 126.42, 125.47, 125.08, 124.14, 123.61, 123.34, 123.05, 122.17, 121.20, 121.12, 120.10, 116.46, 114.96, 49.58, 39.77, 31.97, 31.90, 31.73, 29.95, 29.66, 29.60, 29.38, 26.46, 22.76, 14.24, 14.21. Mass spectrometry (electrospray ionization) (MS (ESI)) m/z calcd. for ($C_{37}H_{42}BrNO$): 595.24. Found: 596.23 ([M + H]$^+$). Anal. Calcd for $C_{37}H_{42}BrNO$: C, 74.48; H, 7.10; N, 2.35. Found: C, 74.45; H, 7.12, N, 2.33%.

10-(4-(Bis(4-(hexyloxy)phenyl)amino)phenyl)-1-(2-hexyldecyl)-1*H*-phenanthro[1,10,9,8-*cdefg*]carbazole-3-carbaldehyde (4). **2** (300 mg, 0.50 mmol), **3** (261 mg, 0.50 mmol), $Pd(OAc)_2$ (3 mg, 0.01 mmol), SPhos (6 mg, 0.01 mmol), K_3PO_4 (530 mg, 2.50 mmol), and dioxane/H_2O (v/v, 5/1, 10 mL) were added to a three-neck round-bottom flask under argon. The reaction mixture was

dx.doi.org/10.1021/am507261j | ACS Appl. Mater. Interfaces 2015, 7, 801−809

refluxed for 8 h and then cooled to room temperature. The resultant mixture was extracted three times with chloroform before the organic phase was washed with water and dried over anhydrous sodium sulfate. After solvent removal under reduced pressure, the residue was purified by column chromatography over silica gel with toluene/petroleum ether (v/v, 1/2) as eluent to afford a red oil as the desired product **4** (400 mg, 83% yield). ^{1}H NMR (400 MHz, THF-d_8) δ: 10.27 (s, 1H), 9.21 (d, J = 8.2 Hz, 1H), 8.65 (d, J = 7.6 Hz, 1H), 8.60 (d, J = 7.6 Hz, 1H), 8.21 (d, J = 8.2 Hz, 1H), 7.98 (s, 1H), 7.79 (m, 1H), 7.73 (m, 1H), 7.64 (s, 1H), 7.53 (d, J = 7.0 Hz, 2H), 7.17 (d, J = 8.9 Hz, 4H), 7.12 (d, J = 8.6 Hz, 2H), 6.90 (d, J = 8.9 Hz, 4H), 4.29 (d, J = 7.4 Hz, 2H), 3.95 (t, J = 6.4 Hz, 4H), 2.15 (m, 1H), 1.77 (m, 4H), 1.50 (m, 4H), 1.36 (m, 10H), 1.28 (m, 6H), 1.12 (m, 16H), 0.91 (m, 6H), 0.77 (m, 6H). ^{13}C NMR (100 MHz, THF-d_8) δ: 192.70, 157.11, 149.65, 141.79, 136.35, 134.12, 131.73, 131.51, 131.19, 131.10, 129.97, 128.81, 127.89, 127.45, 125.97, 125.69, 125.40, 125.23, 125.09, 122.88, 122.03, 121.87, 120.83, 116.44, 116.30, 114.57, 68.96, 50.47, 40.74, 32.92, 32.85, 32.76, 32.70, 32.65, 30.97, 30.69, 30.54, 30.49, 30.33, 27.36, 26.93, 23.71, 23.62, 14.60. MS (ESI) m/z calcd. for ($C_{67}H_{80}N_2O_3$): 960.61. Found: 961.62 ([M + H]$^+$). Anal. Calcd for $C_{67}H_{80}N_2O_3$: C, 83.71; H, 8.39; N, 2.91. Found: C, 83.72; H, 8.42, N, 2.90%.

3-(10-(4-(Bis(4-(hexyloxy)phenyl)amino)phenyl)-1-(2-hexyldecyl)-1*H*-phenanthro[1,10,9,8-*cdefg*]carbazol-3-yl)-2-cyanoacrylic acid (C266). **4** (400 mg, 0.42 mmol), cyanoacetic acid (353 mg, 4.15 mmol), and ammonium acetate (34 mg, 0.42 mmol) were dissolved in acetonitrile/chloroform (v/v, 1/2, 20 mL) in a three-neck round-bottom flask. The reaction mixture was refluxed under argon for 48 h and then cooled to room temperature. Chloroform (30 mL) was added before the organic phase was washed with 0.2 M hydrochloric acid aqueous solution and water in turn and then dried over anhydrous sodium sulfate. After removing the solvent under reduced pressure, the crude product was purified by column chromatography over silica gel with chloroform/methanol (v/v, 15/1) as eluent to afford a black powder as the desired product **C266** (410 mg, 95% yield). ^{1}H NMR (400 MHz, THF-d_8) δ: 9.20 (s, 1H), 8.69 (m, 2H), 8.63 (d, J = 7.6 Hz, 1H), 8.22 (m, 2H), 7.78 (m, 2H), 7.61 (s, 1H), 7.51 (d, J = 8.4 Hz, 2H), 7.15 (d, J = 8.9 Hz, 4H), 7.10 (d, J = 8.4 Hz, 2H), 6.90 (d, J = 8.9 Hz, 4H), 4.22 (m, 2H), 3.96 (t, J = 6.4 Hz, 4H), 2.16 (m, 1H), 1.77 (m, 4H), 1.50 (m, 4H), 1.36 (m, 10H), 1.28 (m, 10H), 1.12 (m, 12H), 0.93 (m, 6H), 0.77 (m, 6H). ^{13}C NMR (100 MHz, THF-d_8) δ: 157.09, 151.09, 149.59, 141.76, 136.30, 134.07, 131.76, 131.64, 131.56, 131.02, 130.68, 129.71, 128.75, 127.92, 126.73, 126.06, 125.69, 125.39, 124.69, 122.93, 121.82, 121.54, 120.79, 118.45, 116.30, 116.07, 114.47, 68.96, 50.44, 40.75, 33.00, 32.92, 32.80, 32.76, 30.95, 30.78, 30.69, 30.50, 30.47, 30.33, 28.17, 27.40, 27.36, 26.93, 23.71, 23.61, 14.59. HR-MS (MALDI) m/z calcd. for ($C_{70}H_{81}N_3O_4$): 1027.6227. Found: 1027.6226 ([M]$^+$). Anal. Calcd for $C_{70}H_{81}N_3O_4$: C, 81.75; H, 7.94; N, 4.09. Found: C, 81.74; H, 7.96, N, 4.11%.

4-(Hexyloxy)-*N*-(4-(hexyloxy)phenyl)-*N*-(4-((triisopropylsilyl)ethynyl)phenyl)aniline (6). **5** (600 mg, 1.16 mmol), (triisopropylsilyl)acetylene (316 mg, 1.74 mmol), Pd(PPh_3)$_2$Cl$_2$ (80 mg, 0.12 mmol), CuI (23 mg, 0.12 mmol), toluene (10 mL), and Et_3N (2 mL) were added to a three-neck round-bottom flask under argon. The reaction mixture was refluxed under argon for 8 h and then cooled to room temperature. The resultant mixture was extracted three times with chloroform before the organic phase was washed with water and dried over anhydrous sodium sulfate. After solvent removal under reduced pressure, the residue was purified by column chromatography over silica gel with ethyl acetate/petroleum ether (v/v, 1/50) as eluent to afford a colorless oil as the desired product **6** (602 mg, 83% yield). ^{1}H NMR (400 MHz, $CDCl_3$) δ: 7.32 (d, J = 8.6 Hz, 2H), 7.08 (d, J = 8.6 Hz, 4H), 6.87 (m, 6H), 3.99 (t, J = 6.5 Hz, 4H), 1.86 (m, 3H), 1.82 (m, 6H), 1.57 (m, 10H), 1.53 (s, 18H), 0.97 (m, 6H). ^{13}C NMR (100 MHz, $CDCl_3$) δ: 157.58, 150.60, 141.69, 134.53, 128.59, 121.06, 117.10, 116.18, 109.59, 90.13, 70.01, 33.31, 31.04, 27.46, 24.30, 20.40, 15.70, 13.15. MS (ESI) m/z calcd. for ($C_{41}H_{59}NO_2Si$): 625.43. Found: 626.44 ([M + H]$^+$). Anal. Calcd for $C_{41}H_{59}NO_2Si$: C, 78.66; H, 9.50; N, 2.24. Found: C, 78.65; H, 9.48, N, 2.26%.

4-Ethynyl-*N*,*N*-bis(4-(hexyloxy)phenyl)aniline (7). **6** (602 mg, 0.96 mmol), tetra-*n*-butylammonium fluoride (2.51 g, 9.60 mmol), and dichloromethane (10 mL) were added to a three-neck round-bottom flask. The reaction mixture was stirred under argon for 3 h at room temperature and then extracted three times with chloroform before the organic phase was washed with water and dried over anhydrous sodium sulfate. After solvent removal under reduced pressure, the residue was used in the subsequent reaction directly.

10-((4-(Bis(4-(hexyloxy)phenyl)amino)phenyl)ethynyl)-1-(2-hexyldecyl)-1*H*-phenanthro[1,10,9,8-*cdefg*]carbazole-3-carbaldehyde (8). **7** (545 mg, 1.16 mmol), **2** (690 mg, 1.16 mmol), Pd(PPh_3)$_2$Cl$_2$ (80 mg, 0.12 mmol), CuI (23 mg, 0.12 mmol), toluene (20 mL), and Et_3N (2 mL) were added to a three-neck round-bottom flask under argon. The reaction mixture was refluxed under argon for 8 h and then cooled to the room temperature. The resultant mixture was extracted three times with chloroform before the organic phase was washed with water and dried over anhydrous sodium sulfate. After solvent removal under reduced pressure, the residue was purified by column chromatography over silica gel with toluene/petroleum ether (v/v, 1/2) as eluent to afford a red oil as the desired product **8** (935 mg, 82% yield). ^{1}H NMR (400 MHz, THF-d_8) δ: 10.35 (s, 1H), 9.21 (d, J = 8.3 Hz, 1H), 8.58 (m, 2H), 8.42 (d, J = 8.1 Hz, 1H), 8.03 (s, 1H), 7.81 (m, 3H), 7.53 (d, J = 8.6 Hz, 2H), 7.11 (d, J = 8.8 Hz, 4H), 6.95 (d, J = 8.6 Hz, 2H), 6.89 (d, J = 8.8 Hz, 4H), 4.28 (d, J = 7.4 Hz, 2H), 3.95 (t, J = 6.4 Hz, 4H), 2.14 (m, 1H), 1.78 (m, 4H), 1.50 (m, 4H), 1.37 (m, 16H), 1.13 (m, 16H), 0.93 (m, 6H), 0.78 (m, 6H). ^{13}C NMR (100 MHz, THF-d_8) δ: 192.84, 157.52, 150.39, 141.03, 135.27, 133.44, 132.44, 130.86, 130.77, 130.70, 129.95, 128.28, 127.78, 127.55, 126.21, 125.30, 125.11, 124.36, 123.10, 122.40, 121.40, 119.89, 117.56, 117.03, 116.34, 115.11, 96.63, 88.93, 68.96, 50.60, 40.78, 32.92, 32.87, 32.75, 30.97, 30.70, 30.55, 30.47, 30.34, 27.40, 26.92, 23.20, 23.62, 14.58. MS (ESI) m/z calcd. for ($C_{69}H_{80}N_2O_3$): 984.62. Found: 985.60 ([M + H]$^+$). Anal. Calcd for $C_{69}H_{80}N_2O_3$: C, 84.10; H, 8.18; N, 2.84. Found: C, 84.11; H, 8.16; N, 2.82%.

3-(10-((4-(Bis(4-(hexyloxy)phenyl)amino)phenyl)ethynyl)-1-(2-hexyldecyl)-1*H*-phenanthro[1,10,9,8-*cdefg*]carbazol-3-yl)-2-cyanoacrylic acid (C267). **8** (935 mg, 0.95 mmol), cyanoacetic acid (807 mg, 9.50 mmol), ammonium acetate (68 mg, 0.95 mmol), and acetonitrile/chloroform (v/v, 1/2, 20 mL) were added to a three-neck round-bottom flask. The reaction mixture was refluxed for 48 h and then cooled to room temperature. Chloroform (30 mL) was added before the organic phase was washed with 0.2 M phosphonic acid aqueous solution and water in turn and then dried over anhydrous sodium sulfate. After removing the solvent under reduced pressure, the crude product was purified by column chromatography over silica gel with chloroform/methanol (v/v, 15/1) as eluent to afford a black powder as the desired product **C267** (959 mg, 96% yield). ^{1}H NMR (400 MHz, THF-d_8) δ: 9.09 (s, 1H), 8.63 (s, 1H), 8.49 (d, J = 7.7 Hz, 1H), 8.43 (d, J = 7.7 Hz, 1H), 8.38 (d, J = 8.1 Hz, 1H), 8.06 (d, J = 8.6 Hz, 1H), 7.72 (m, 1H), 7.69 (m, 1H), 7.74 (s, 1H), 7.55 (d, J = 8.7 Hz, 2H), 7.12 (d, J = 8.9 Hz, 4H), 6.95 (d, J = 8.7 Hz, 2H), 6.89 (d, J = 9.0 Hz, 4H), 4.13 (d, J = 7.5 Hz, 2H), 3.95 (t, J = 6.4 Hz, 4H), 2.08 (m, 1H), 1.79 (m, 4H), 1.50 (m, 4H), 1.37 (m, 14H), 1.11 (m, 18H), 0.93 (m, 6H), 0.77 (m, 6H). ^{13}C NMR (100 MHz, THF-d_8) δ: 165.01, 157.48, 151.44, 150.33, 141.05, 135.30, 133.52, 132.38, 131.86, 130.52, 129.87, 129.52, 128.25, 126.66, 126.21, 125.43, 125.25, 124.45, 124.14, 123.08, 122.11, 121.55, 121.48, 121.42, 119.95, 118.04, 117.36, 116.84, 116.33, 116.10, 115.20, 101.43, 96.88, 89.06, 68.96, 50.64, 40.85, 32.93, 32.82, 32.75, 30.95, 30.78, 30.70, 30.49, 30.47, 30.36, 27.48, 27.44, 26.92, 23.70, 23.63, 14.61, 14.59. HR-MS (MALDI) m/z calcd. for ($C_{72}H_{81}N_3O_4$): 1051.6227. Found: 1051.6225. Anal. Calcd for $C_{72}H_{81}N_3O_4$: C, 82.17; H, 7.76; N, 3.99. Found: C, 82.13; H, 7.73; N, 4.02%.

Computational Details. All the calculations were carried out with Gaussian 09 program packages. The ground-state geometries were optimized employing the hybrid B3LYP function.[64] For the vertical excitation calculations as well as the oscillator strengths (f), we used hybrid functional MPW1K[65] including 42% of Hartree−Fock exchange, which has been demonstrated as a suitable selection for donor−acceptor organic dyes featuring intramolecular charge-transfer

transition.[66] The 6-311G(d, p) basis set was selected for the calculations. The solvent (THF) effects on the geometries and absorption spectra were simulated by the conductor-like polarized continuum model (C-PCM).[67]

Cell Fabrication and Characterization. A bilayer titania film made via screen-printing on a precleaned fluorine-doped tin oxide (FTO) conducting glass (Nippon Sheet Glass, Solar, 4 mm thick) was employed as the negative electrode of DSCs presented in this paper. A 4.2 μm thick translucent layer of 25 nm sized titania particles was first deposited on a FTO glass and further covered with a 5.0 μm thick light-scattering layer of 350−450 nm sized titania particles (WER4-O, Dyesol). Preparation procedures of titania nanocrystals, screen-printing pastes, and nanostructured titania films were very similar to those described in a previous paper.[68] A circular titania electrode (~0.28 cm^2) was dye-loaded by immersing it into a 150 μM dye solution with chloroform/ethanol (v/v, 1/19) as the dye-bath solvent for 12 h. The dye-grafted titania electrode was assembled with a gold-coated FTO electrode by use of a 25 μm thick Surlyn ring to produce a thin-layer electrochemical cell. The infiltrated Co-bpy electrolyte is composed of 0.25 M tris(2,2′-bipyridine)cobalt(II) di[bis-(trifluoromethanesulfonyl)imide], 0.05 M tris(2,2′-bipyridine)cobalt-(III) tris[bis(trifluoromethanesulfonyl)imide], 0.5 M *t*BP, and 0.1 M lithium bis(trifluoromethanesulfonyl)imide (LiTFSI) in acetonitrile. Details on EQE, *J*−*V*, CE, and TPD measurements have been described in our previous works.[69,70]

Voltammetric, UV−vis, and XRR Measurements. Cyclic voltammograms of the dye solutions were recorded on a CHI660C electrochemical workstation, and all potentials were reported with respect to the ferrocene (Fc) reference. Electronic absorption measurements were carried out on an Agilent G1103A spectrometer. For the spectroscopic measurements of dye-grafted oxide films, we utilized one dyed, translucent layer of nanostructured titania film deposited on FTO in conjunction with another bare FTO to make the Co-bpy electrolyte-filled samples by use of the same protocol for DSC fabrication. XRR measurements were carried out with a Bruker D8 discover high-resolution diffractometer by using Cu Kα X-ray radiation (λ = 1.542 Å), and the experimental details have been described in our pervious paper.[62]

■ ASSOCIATED CONTENT

Supporting Information

PL data, detailed parameters derived from XRR, and NMR spectra of **2**, **4**, **6**, **8**, **C266**, and **C267**. This material is available free of charge via the Internet at http://pubs.acs.org.

■ AUTHOR INFORMATION

Corresponding Authors

*E-mail: minzhang@ciac.ac.cn. Phone: 0086-431-85262952. (M.Z.)

*E-mail: peng.wang@ciac.ac.cn. (P.W.)

Notes

The authors declare no competing financial interest.

■ ACKNOWLEDGMENTS

Acknowledgements are made to the National 973 Program (2011CBA00702 and 2015CB932204), the National 863 Program (2011AA050521), and the National Science Foundation of China (51125015, 91233206, and 51473158) for financial support.

■ REFERENCES

(1) O'Regan, B.; Grätzel, M. A Low-Cost, High-Efficiency Solar Cell Based on Dye-Sensitized Colloidal TiO_2 Films. *Nature* **1991**, *353*, 737−740.

(2) Ozawa, H.; Okuyama, Y.; Arakawa, H. Dependence of the Efficiency Improvement of Black-Dye-Based Dye-Sensitized Solar Cells on Alkyl Chain Length of Quaternary Ammonium Cations in Electrolyte Solutions. *ChemPhysChem* **2014**, *15*, 1201−1206.

(3) Mathew, S.; Yella, A.; Gao, P.; Humphry-Baker, R.; Curchod, B. F. E.; Ashari-Astani, N.; Tavernelli, I.; Rothlisberger, U.; Nazeeruddin, M. K.; Grätzel, M. Dye-Sensitized Solar Cells with 13% Efficiency Achieved through the Molecular Engineering of Porphyrin Sensitizers. *Nat. Chem.* **2014**, *6*, 242−247.

(4) Kakiage, K.; Aoyama, Y.; Yano, T.; Otsuka, T.; Kyomen, T.; Unno, M.; Hanaya, M. An Achievement of Over 12% Efficiency in an Organic Dye-Sensitized Solar Cell. *Chem. Commun.* **2014**, *50*, 6379−6381.

(5) Hara, K.; Kurashige, M.; Dan-oh, Y.; Kasada, C.; Shinpo, A.; Suga, S.; Sayama, K.; Arakawa, H. Design of New Coumarin Dyes Having Thiophene Moieties for Highly Efficient Organic-Dye-Sensitized Solar Cells. *New J. Chem.* **2003**, *27*, 783−785.

(6) Horiuchi, T.; Miura, H.; Sumioka, K.; Uchida, S. High Efficiency of Dye-Sensitized Solar Cells Based on Metal-Free Indoline Dyes. *J. Am. Chem. Soc.* **2004**, *126*, 12218−12219.

(7) Velusamy, M.; Thomas, K. R. J.; Lin, J. T.; Hsu, Y.-C.; Ho, K.-C. *Org. Lett.* **2005**, *7*, 1899−1902.

(8) Hara, K.; Wang, Z.-S.; Sato, T.; Furube, A.; Katoh, R.; Sugihara, H.; Dan-oh, Y.; Kasada, C.; Shinpo, A.; Suga, S. Oligothiophene-Containing Coumarin Dyes for Efficient Dye-Sensitized Solar Cells. *J. Phys. Chem. B* **2005**, *109*, 15476−15482.

(9) Hagberg, D. P.; Edvinsson, T.; Marinado, T.; Boschloo, G.; Hagfeldt, A.; Sun, L. A Novel Organic Chromophore for Dye-Sensitized Nanostructured Solar Cells. *Chem. Commun.* **2006**, 2245−2247.

(10) Li, S.-L.; Jiang, K.-J.; Shao, K.-F.; Yang, L.-M. Novel Organic Dyes for Efficient Dye-Sensitized Solar Cells. *Chem. Commun.* **2006**, 2792−2794.

(11) Koumura, N.; Wang, Z.-S.; Mori, S.; Miyashita, M.; Suzuki, E.; Hara, K. Alkyl-Functionalized Organic Dyes for Efficient Molecular Photovoltaics. *J. Am. Chem. Soc.* **2006**, *128*, 14256−14257.

(12) Burke, A.; Schmidt-Mende, L.; Ito, S.; Grätzel, M. A Novel Blue Dye for Near-IR 'Dye-Sensitised' Solar Cell Applications. *Chem. Commun.* **2007**, 234−236.

(13) Thomas, K. R. J.; Hsu, Y.-C.; Lin, J. T.; Lee, K.-M.; Ho, K.-C.; Lai, C.-H.; Cheng, Y.-M.; Chou, P.-T. 2,3-Disubstituted Thiophene-Based Organic Dyes for Solar Cells. *Chem. Mater.* **2008**, *20*, 1830−1840.

(14) Imahori, H.; Umeyama, T.; Ito, S. Large π-Aromatic Molecules as Potential Sensitizers for Highly Efficient Dye-Sensitized Solar Cells. *Acc. Chem. Res.* **2009**, *42*, 1809−1818.

(15) Mishra, A.; Fischer, M. K. R.; Bäuerle, P. Metal-Free Organic Dyes for Dye-Sensitized Solar Cells: From Structure: Property Relationships to Design Rules. *Angew. Chem., Int. Ed.* **2009**, *48*, 2474−2499.

(16) Ji, Z.; Natu, G.; Huang, Z.; Wu, Y. Linker Effect in Organic Donor−Acceptor Dyes for p-Type NiO Dye Sensitized Solar Cells. *Energy Environ. Sci.* **2011**, *4*, 2818−2821.

(17) Bai, Y.; Zhang, J.; Zhou, D.; Wang, Y.; Zhang, M.; Wang, P. Engineering Organic Sensitizers for Iodine-Free Dye-Sensitized Solar Cells: Red-Shifted Current Response Concomitant with Attenuated Charge Recombination. *J. Am. Chem. Soc.* **2011**, *133*, 11442−11445.

(18) Daeneke, T.; Kwon, T.-H.; Holmes, A. B.; Duffy, N. W.; Bach, U.; Spiccia, L. High-Efficiency Dye-Sensitized Solar Cells with Ferrocene-Based Electrolytes. *Nat. Chem.* **2011**, *3*, 211−215.

(19) Zhu, W.; Wu, Y.; Wang, S.; Li, W.; Li, X.; Chen, J.; Wang, Z.-S.; Tian, H. Organic D-A-π-A Solar Cell Sensitizers with Improved Stability and Spectral Response. *Adv. Funct. Mater.* **2011**, *21*, 756−763.

(20) Chen, J.-H.; Tsai, C.-H.; Wang, S.-A.; Lin, Y.-Y.; Huang, T.-W.; Chiu, S.-F.; Wu, C.-C.; Wong, K.-T. Organic Dyes Containing a Coplanar Indacenodithiophene Bridge for High-Performance Dye-Sensitized Solar Cells. *J. Org. Chem.* **2011**, *76*, 8977−8985.

(21) Mathew, S.; Imahori, H. Tunable, Strongly-Donating Perylene Photosensitizers for Dye-Sensitized Solar Cells. *J. Mater. Chem.* **2011**, *21*, 7166−7174.

(22) Chen, Y.-C.; Chou, H.-H.; Tsai, M. C.; Chen, S.-Y.; Lin, J. T.; Yao, C.-F.; Chen, K. Thieno[3,4-*b*]thiophene-Based Organic Dyes for Dye-Sensitized Solar Cells. *Chem.—Eur. J.* **2012**, *18*, 5430−5437.
(23) Li, C.; Wonneberger, H. Perylene Imides for Organic Photovoltaics: Yesterday, Today, and Tomorrow. *Adv. Mater.* **2012**, *24*, 613−636.
(24) Do, K.; Kim, D.; Cho, N.; Paek, S.; Song, K.; Ko, J. New Type of Organic Sensitizers with a Planar Amine Unit for Efficient Dye-Sensitized Solar Cells. *Org. Lett.* **2012**, *14*, 222−225.
(25) Zhang, M.; Wang, Y.; Xu, M.; Ma, W.; Li, R.; Wang, P. Design of High-Efficiency Organic Dyes for Titania Solar Cells Based on the Chromophoric Core of Cyclopentadithiophene-Benzothiadiazole. *Energy Environ. Sci.* **2013**, *6*, 2944−2949.
(26) Cai, N.; Li, R.; Wang, Y.; Zhang, M.; Wang, P. Organic Dye-Sensitized Solar Cells with a Cobalt Redox Couple: Influences of π-Linker Rigidification and Dye−Bath Solvent Selection. *Energy Environ. Sci.* **2013**, *6*, 139−147.
(27) Yao, Z.; Yang, L.; Cai, Y.; Yan, C.; Zhang, M.; Cai, N.; Dong, X.; Wang, P. Rigidifying the π-Linker to Enhance Light Absorption of Organic Dye-Sensitized Solar Cells and Influences on Charge Transfer Dynamics. *J. Phys. Chem. C* **2014**, *118*, 2977−2986.
(28) Würther, F. Perylene Bisimide Dyes as Versatile Building Blocks for Functional Supramolecular Architectures. *Chem. Commun.* **2004**, 1564−1579.
(29) Tang, C. W. Two-Layer Organic Photovoltaic Cell. *Appl. Phys. Lett.* **1986**, *48*, 183−185.
(30) Schmidt-Mende, L.; Fechtenkötter, A.; Müllen, K.; Moons, E.; Friend, R. H.; MacKenzie, J. D. Self-Organized Discotic Liquid Crystals for High-Efficiency Organic Photovoltaics. *Science* **2001**, *293*, 1119−1122.
(31) Peumans, P.; Uchida, S.; Forrest, S. R. Efficient Bulk Heterojunction Photovoltaic Cells Using Small-Molecular-Weight Organic Thin Films. *Nature* **2003**, *425*, 158−162.
(32) Ferrere, S.; Gregg, B. A. New Perylenes for Dye Sensitization of TiO_2. *New J. Chem.* **2002**, *26*, 1155−1160.
(33) Shibano, Y.; Umeyama, T.; Matano, Y.; Imahori, H. Electron-Donating Perylene Tetracarboxylic Acids for Dye-Sensitized Solar Cells. *Org. Lett.* **2007**, *9*, 1971−1974.
(34) Zafer, C.; Kus, M.; Turkmen, G.; Dincalp, H.; Demic, S.; Kuban, B.; Teoman, Y.; Icli, S. New Perylene Derivative Dyes for Dye-Sensitized Solar Cells. *Sol. Energy Mater. Sol. Cells* **2007**, *91*, 427−431.
(35) Edvinsson, T.; Li, C.; Pschirer, N.; Schöneboom, J.; Eickemeyer, F.; Sens, R.; Boschloo, G.; Herrmann, A.; Müllen, K.; Hagfeldt, A. Intramolecular Charge-Transfer Tuning of Perylenes: Spectroscopic Features and Performance in Dye-Sensitized Solar Cells. *J. Phys. Chem. C* **2007**, *111*, 15137−15140.
(36) Fortage, J.; Séverac, M.; Houarner-Rassin, C.; Pellegrin, Y.; Blart, E.; Odobel, F. Synthesis of New Perylene Imide Dyes and Their Photovoltaic Performances in Nanocrystalline TiO_2 Dye-Sensitized Solar Cells. *J. Photochem. Photobiol., A* **2008**, *197*, 156−169.
(37) Jin, Y.; Hua, J.; Wu, W.; Ma, X.; Meng, F. Synthesis, Characterization and Photovoltaic Properties of Two Novel Near-Infrared Absorbing Perylene Dyes Containing Benzo[*e*]indole for Dye-Sensitized Solar Cells. *Synth. Met.* **2008**, *158*, 64−71.
(38) Li, C.; Yum, J.-H.; Moon, S.-J.; Herrmann, A.; Eickemeyer, F.; Pschirer, N. G.; Erk, P.; Schöneboom, J.; Müllen, K.; Grätzel, M.; Nazeeruddin, M. K. An Improved Perylene Sensitizer for Solar Cell Applications. *ChemSusChem* **2008**, *1*, 615−618.
(39) Cappel, U. B.; Karlsson, M. H.; Pschirer, N. G.; Eickemeyer, F.; Schöneboom, J.; Erk, P.; Boschloo, G.; Hagfeldt, A. A Broadly Absorbing Perylene Dye for Solid-State Dye-Sensitized Solar Cells. *J. Phys. Chem. C* **2009**, *113*, 14595−14597.
(40) Li, C.; Liu, Z.; Schöneboom, J.; Eickemeyer, F.; Pschirer, N. G.; Erk, P.; Herrmann, A.; Müllen, K. Perylenes as Sensitizers in Hybrid Solar Cells: How Molecular Size Influences Performance. *J. Mater. Chem.* **2009**, *19*, 5405−5415.
(41) Pleux, L. L.; Smeigh, A. L.; Gibson, E.; Pellegrin, Y.; Blart, E.; Boschloo, G.; Hagfeldt, A.; Hammarström, L.; Odobe, F. Synthesis, Photophysical and Photovoltaic Investigations of Acceptor-Functionalized Perylene Monoimide Dyes for Nickel Oxide p-Type Dye-Sensitized Solar Cells. *Energy Environ. Sci.* **2011**, *4*, 2075−2084.
(42) Keerthi, A.; Liu, Y.; Wang, Q.; Valiyaveettil, S. Synthesis of Perylene Dyes with Multiple Triphenylamine Substituents. *Chem.—Eur. J.* **2012**, *18*, 11669−11676.
(43) Zhang, M.; Yao, Z.; Yan, C.; Cai, Y.; Ren, Y.; Zhang, J.; Wang, P. Unraveling the Pivotal Impacts of Electron-Acceptor on Light Absorption and Carrier Photogeneration in Perylene Dye Sensitized Solar Cells. *ACS Photonics* **2014**, *1*, 710−717.
(44) Langhals, H.; Christian, S.; Hofer, A. Substitution of Aromatics by Amines at Room Temperature with Negative Energy of Activation: Amino *peri*-Arylenes as Metal-Free Components for Dye-Sensitized Solar Cells. *J. Org. Chem.* **2013**, *78*, 9883−9891.
(45) Luo, J.; Xu, M.; Li, R.; Huang, K.-W.; Jiang, C.; Qi, Q.; Zeng, W.; Zhang, J.; Chi, C.; Wang, P.; Wu, J. *N*-Annulated Perylene as an Efficient Electron Donor for Porphyrin-Based Dyes: Enhanced Light-Harvesting Ability and High-Efficiency Co(II/III)-Based Dye-Sensitized Solar Cells. *J. Am. Chem. Soc.* **2014**, *136*, 265−272.
(46) Yao, Z.; Yan, C.; Zhang, M.; Li, R.; Cai, Y.; Wang, P. *N*-Annulated Perylene as a Coplanar π-Linker Alternative to Benzene as a Low Energy-Gap, Metal-Free Dye in Sensitized Solar Cells. *Adv. Energy Mater.* **2014**, *4*, 1400244.
(47) Ferrere, S.; Zaban, A.; Gregg, B. A. Dye Sensitization of Nanocrystalline Tin Oxide by Perylene Derivatives. *J. Phys. Chem. B* **1997**, *101*, 4490−4493.
(48) Teng, C.; Yang, X.; Yang, C.; Tian, H.; Li, S.; Wang, X.; Hagfeldt, A.; Sun, L. Influence of Triple Bonds as π-Spacer Units in Metal-Free Organic Dyes for Dye-Sensitized Solar Cells. *J. Phys. Chem. C* **2010**, *114*, 11305−11313.
(49) Katono, M.; Bessho, T.; Wielopolski, M.; Marszalek, M.; Moser, J.-E.; Humphry-Baker, R.; Zakeeruddin, S. M.; Grätzel, M. Influence of the Anchoring Modes on the Electronic and Photovoltaic Properties of D−π−A Dyes. *J. Phys. Chem. C* **2012**, *116*, 16876−16884.
(50) Lee, C.-W.; Lu, H.-P.; Lan, C.-M.; Huang, Y.-L.; Liang, Y.-R.; Yen, W.-N.; Liu, Y.-C.; Lin, Y.-S.; Diau, E. W.-G.; Yeh, C.-Y. Novel Zinc Porphyrin Sensitizers for Dye-Sensitized Solar Cells: Synthesis and Spectral, Electrochemical, and Photovoltaic Properties. *Chem.—Eur. J.* **2009**, *15*, 1403−1412.
(51) Kurotobi, K.; Toude, Y.; Kawamoto, K.; Fujimori, Y.; Ito, S.; Chabera, P.; Sundström, V.; Imahori, H. Highly Asymmetrical Porphyrins with Enhanced Push−Pull Character for Dye-Sensitized Solar Cells. *Chem.—Eur. J.* **2013**, *19*, 17075−17081.
(52) Li, R.; Liu, J.; Cai, N.; Zhang, M.; Wang, P. Synchronously Reduced Surface States, Charge Recombination, and Light Absorption Length for High-Performance Organic Dye-Sensitized Solar Cells. *J. Phys. Chem. B* **2010**, *114*, 4461−4464.
(53) Walker, S. D.; Barder, T. E.; Martinelli, J. R.; Buchwald, S. L. A Rationally Designed Universal Catalyst for Suzuki−Miyaura Coupling Processes. *Angew. Chem., Int. Ed.* **2004**, *43*, 1871−1876.
(54) Bisquert, J. Chemical Capacitance of Nanostructured Semiconductors: Its Origin and Significance for Nanocomposite Solar Cells. *Phys. Chem. Chem. Phys.* **2003**, *5*, 5360−5364.
(55) O'Regan, B. C.; Durrant, J. R. Kinetic and Energetic Paradigms for Dye-Sensitized Solar Cells: Moving from the Ideal to the Real. *Acc. Chem. Res.* **2009**, *42*, 1799−1808.
(56) Duffy, N.W.; Peter, L. M.; Rajapakse, R. M. G.; Wijayant, K. G. U. A Novel Charge Extraction Method for the Study of Electron Transport and Interfacial Transfer in Dye Sensitised Nanocrystalline Solar Cells. *Electrochem. Commun.* **2000**, *2*, 658−662.
(57) O'Regan, B. C.; Bakker, K.; Kroeze, J.; Smit, H.; Sommeling, P.; Durrant, J. R. Measuring Charge Transport from Transient Photovoltage Rise Times. A New Tool to Investigate Electron Transport in Nanoparticle Films. *J. Phys. Chem. B* **2006**, *110*, 17155−17160.
(58) Schlichthorl, G.; Huang, S.; Sprague, J.; Frank, A. J. Band Edge Movement and Recombination Kinetics in Dye-Sensitized Nanocrystalline TiO_2 Solar Cells: A Study by Intensity Modulated Photovoltage Spectroscopy. *J. Phys. Chem. B* **1997**, *101*, 8141−8155.
(59) Decher, G. Nanoassemblies: Toward Layered Polymeric Multicomposites. *Science* **1997**, *277*, 1232−1237.

(60) Daillant, J.; Gihaud, A. *X-ray and Neutron Reflectivity: Principles and Applications;* Springer-Verlag: Berlin, 2009.
(61) Griffith, M. J.; James, M.; Triani, G.; Wagner, P.; Wallace, G. G.; Officer, D. L. Determining the Orientation and Molecular Packing of Organic Dyes on a TiO_2 Surface Using X-ray Reflectometry. *Langmuir* **2011**, *27*, 12944−12950.
(62) Zhang, M.; Zhang, J.; Fan, Y.; Yang, L.; Wang, Y.; Li, R.; Wang, P. Judicious Selection of a Pinhole Defect Filler to Generally Enhance the Performance of Organic Dye-Sensitized Solar Cells. *Energy Environ. Sci.* **2013**, *6*, 2939−2943.
(63) Jiang, W.; Qian, H.; Li, Y.; Wang, Z. Heteroatom-Annulated Perylenes: Practical Synthesis, Photophysical Properties, and Solid-State Packing Arrangement. *J. Org. Chem.* **2008**, *73*, 7369−7372.
(64) Lee, C.; Yang, W.; Parr, R. G. Development of the Colle-Salvetti Correlation-Energy Formula into a Functional of the Electron Density. *Phys. Rev. B* **1988**, *37*, 785−789.
(65) Lynch, B. J.; Fast, P. L.; Harris, M.; Truhlar, D. G. A Adiabatic Connection for Kinetic. *J. Phys. Chem. A* **2000**, *104*, 4811−4813.
(66) Pastore, M.; Mosconi, E.; De Angelis, F.; Gätzel, M. A Computational Investigation of Organic Dyes for Dye-Sensitized Solar Cells: Benchmark, Strategies, and Open Issues. *J. Phys. Chem. C* **2010**, *114*, 7205−7212.
(67) Cossi, M.; Rega, N.; Scalmani, G.; Barone, V. Energies, Structures, and Electronic Properties of Molecules in Solution with the C-PCM Solvation Model. *J. Comput. Chem.* **2003**, *24*, 669−681.
(68) Wang, P.; Zakeeruddin, S. M.; Comte, P.; Charvet, R.; Humphry-Baker, R.; Grätzel, M. Enhance the Performance of Dye-Sensitized Solar Cells by Co-grafting Amphiphilic Sensitizer and Hexadecylmalonic Acid on TiO_2 Nanocrystals. *J. Phys. Chem. B* **2003**, *107*, 14336−14341.
(69) Liu, J.; Li, R.; Si, X.; Zhou, D.; Shi, Y.; Wang, Y.; Wang, P. Oligothiophene Dye-Sensitized Solar Cells. *Energy Environ. Sci.* **2010**, *3*, 1924−1928.
(70) Cai, N.; Wang, Y.; Xu, M.; Fan, Y.; Li, R.; Zhang, M.; Wang, P. Engineering of Push-Pull Thiophene Dyes to Enhance Light Absorption and Modulate Charge Recombination in Mesoscopic Solar Cells. *Adv. Funct. Mater.* **2013**, *23*, 1846−1854.